Effect of Soil Properties on Electromagnetic Radiation Penetration

TABLE OF CONTENTS

ABSTRACT

For humanitarian demining purposes we are aiming to design a system for the remote detection and neutralization of landmines, using high power microwaves. In this project we will study the effect of the soil on the incident EM waves. The rise of temperature in the soil will be studied due to the exposure of microwaves, for the neutralization process. And the best way to deliver power for a fast raise in temperature. In addition, we will design a GPR (ground penetrating radar) to probe underneath the soil, and run simulations to collect data belonging to different targets and shapes, and feed the recognition system with these data.

The software used for the simulations is CST Microwave studio.

RESUME

Servant le déminage humanitaire, on va essayer d'élaborer un système pour la détection et neutralisation des mines, en utilisant des microondes à haute puissance. Dans ce projet on étudiera l'impact des propriétés du sol sur la pénétration des radiations électromagnétiques. L'élévation en température dans le sol doit être étudiée lorsqu'il est exposé aux microondes, pour la neutralisation des mines. En plus, on devra construire un radar à pénétration de sol (RPS) pour sonder tous ce qu'il est au-dessous du sol, et lancer des simulations pour collecter des données appartenant au différents objet a différents formes, et ensuite fournir ces données à la système de reconnaissance.

Le logicielle utilisée dans notre simulations est le CST Microwave studio.

CHAPTER 0: INTRODUCTION

1. Background

During the late 1900's, military forces and civilians around the world, suffered a large number of landmines accidents. Many of these accidents involved vehicles that were struck by landmines buried in roads. Which made this topic a target for researches and studies by military forces and universities around the world.

A solution was found for the detection of landmines, by using the magnetic field to detect metals underground and thus pinpointing the landmines and detection their exact position.

In the early 1990's the metal detectors start showing failure in detecting landmines with low metal content, and that leaded to many accidents.

Therefore the ultimate goal of our project is to design an integrated technologically-advanced system for the remote detection, localization, and neutralization of landmines. The advantages of such a system would be the faster, more secure, and less expensive demining efforts.

This project

This specific project has to do with the effect of soil on electromagnetic radiation penetration, especially in the applications of GPR and landmine neutralization using high power microwaves.

The other parts of the project would be done separately but we will be in contact with the recognition part due to the data exchange.

For the soil properties, previous studies were made to extract the electrical properties of different types of soil and in different conditions, we are going to use the results of these studies in our simulations.

Studies were also made on ground penetrating radars but to probe the earth for long depths in order to detect water and rock beds deeply underground for archeological purposes, and using seismic waves.

In the following we will study the power attenuation in the soil and find the best way to deliver enough amount of power for the landmines neutralization, then we will design and simulate a ground penetrating radar and study the possibility of creating an efficient recognition system that could be able to distinguish between landmines and other buried objects, or even between different types of landmines.

All the simulation done in this project are ran in CST microwaves studio®, a specialist tool for the 3D EM simulation of high frequency components.

CHAPTER I: STATE OF ART

1. Ground penetrating radar

Ground-penetrating radar (GPR) uses a high-frequency EM pulse transmitted from a radar antenna to probe the earth. The pulse is transmitted into the ground, and is returned to the surface as a series of reflections from discontinuities at depth. The reflected energy is received at one or more locations along the ground surface. Data are collected as reflected energy versus time, and converted to depth using knowledge of the propagation velocity within the soil.

The resolving power for reflection imaging is limited by the wavelength of the energy source, which is controlled by the wave frequency and propagation velocity. Attenuation and scattering increase for short wavelength energy, placing practical limits on the highest frequencies that may be used, and therefore, on the overall imaging resolution.

Ground-penetrating radar uses radio frequency electromagnetic waves as an energy source, which are sensitive to the dielectric properties of the soil and reflective objects within it.

The GPR is usually used in the earth sciences to study bedrock, soils, groundwater, and ice, or in archaeology. And that requires the usage of big wavelength (in meters) to reach deep places.

In this project we don't need to study deeper than 30cm underground, so we can adapt the frequency to get better resolution, but taking into consideration the limitations.

To construct images of the subsurface reflectors, the sources and receivers are moved along the ground surface.

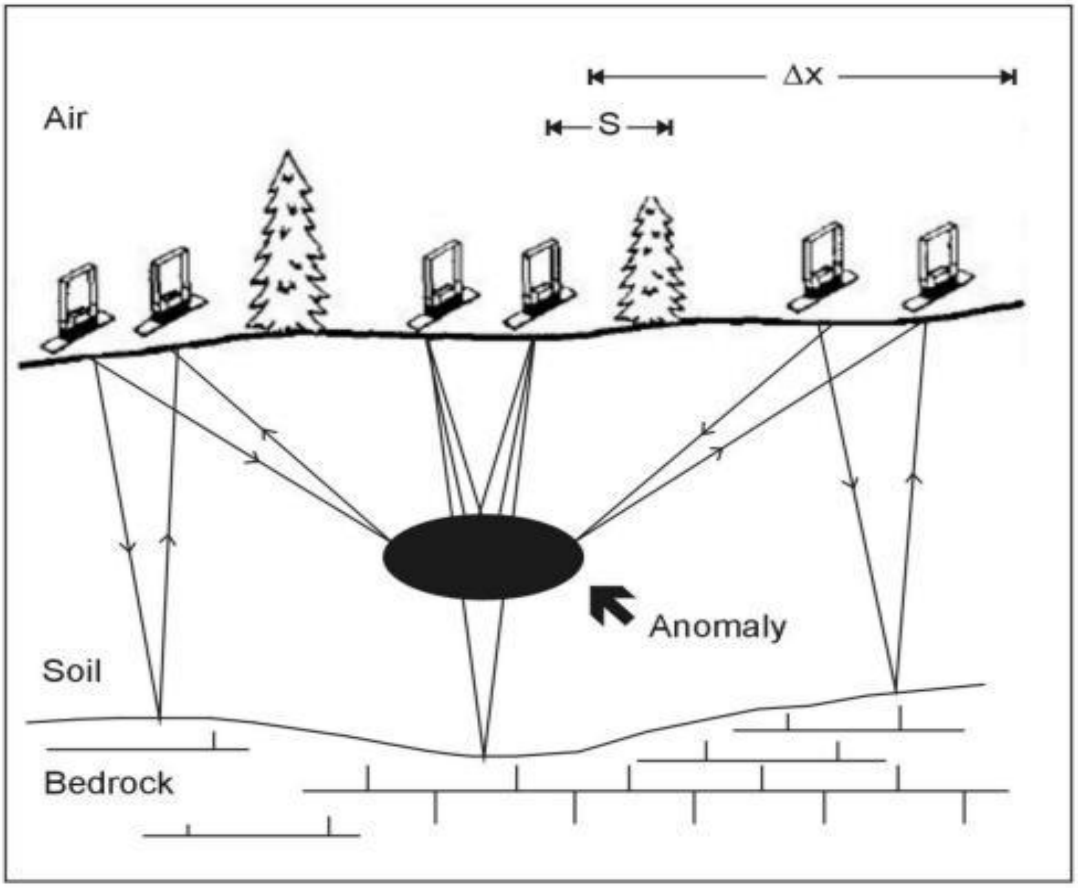

Fig.1 GPR system

Reflectors may be soil horizons, the groundwater surface, soil/rock interfaces, man-made objects, or any other interface having a contrast in dielectric properties.

The signal collected at the receiver at each step is gathered and processed to form an underground image of the soil section.

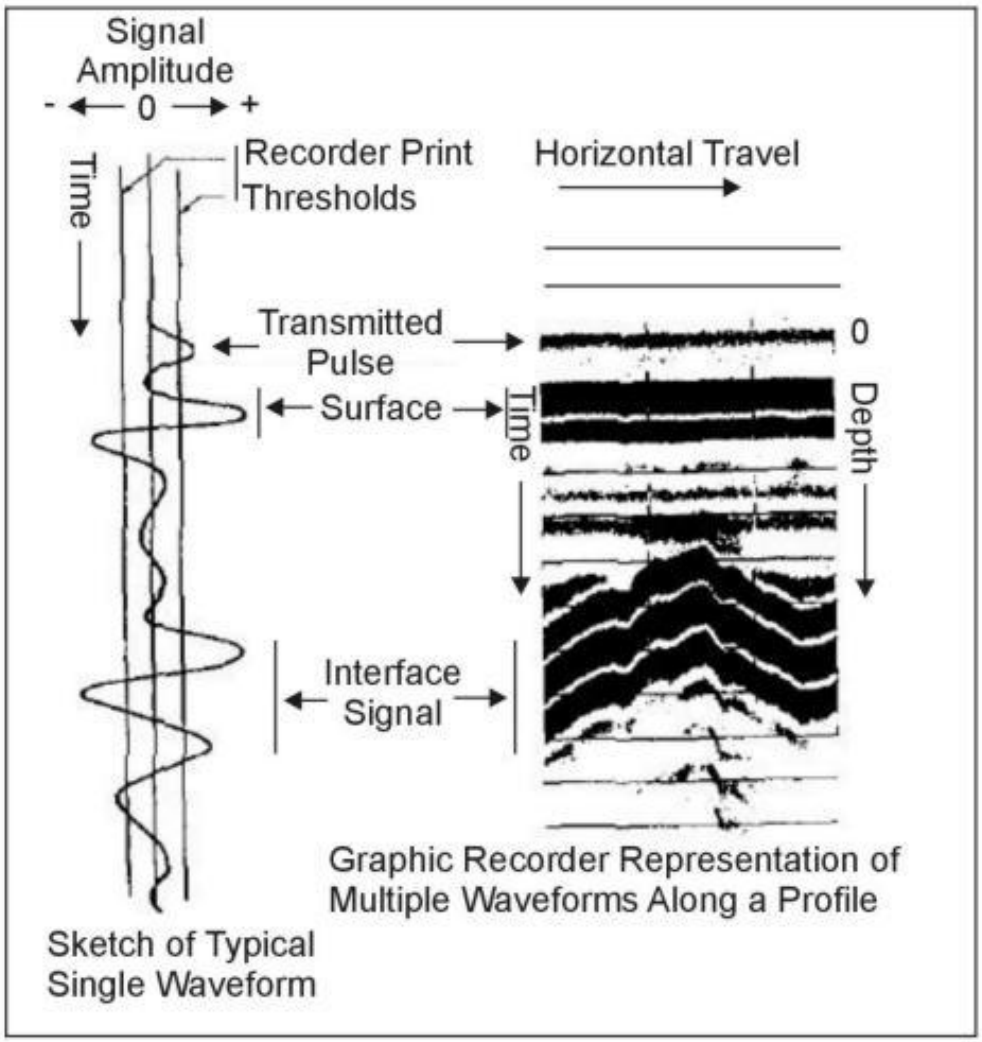

Fig.2 Data collected from GPR

The image constructed in the figure above is not a real image showing what is underground, it actually shows interfered hyperbolic shapes. The reflectors are seen as hyperbolic shapes due to the uniform linear movement of the radar, to reconstruct the real image we have to use an algorithm called migration.

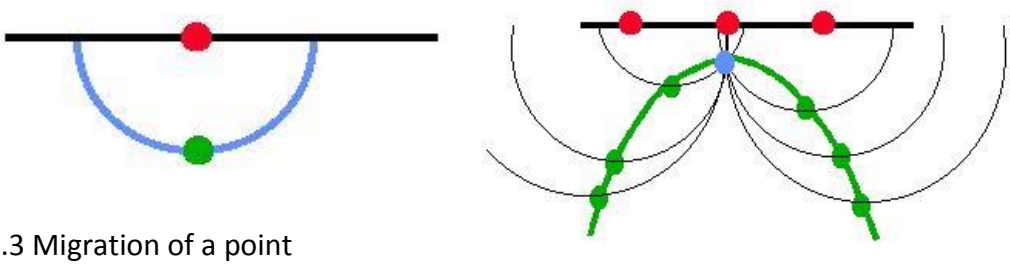

Fig.3 Migration of a point

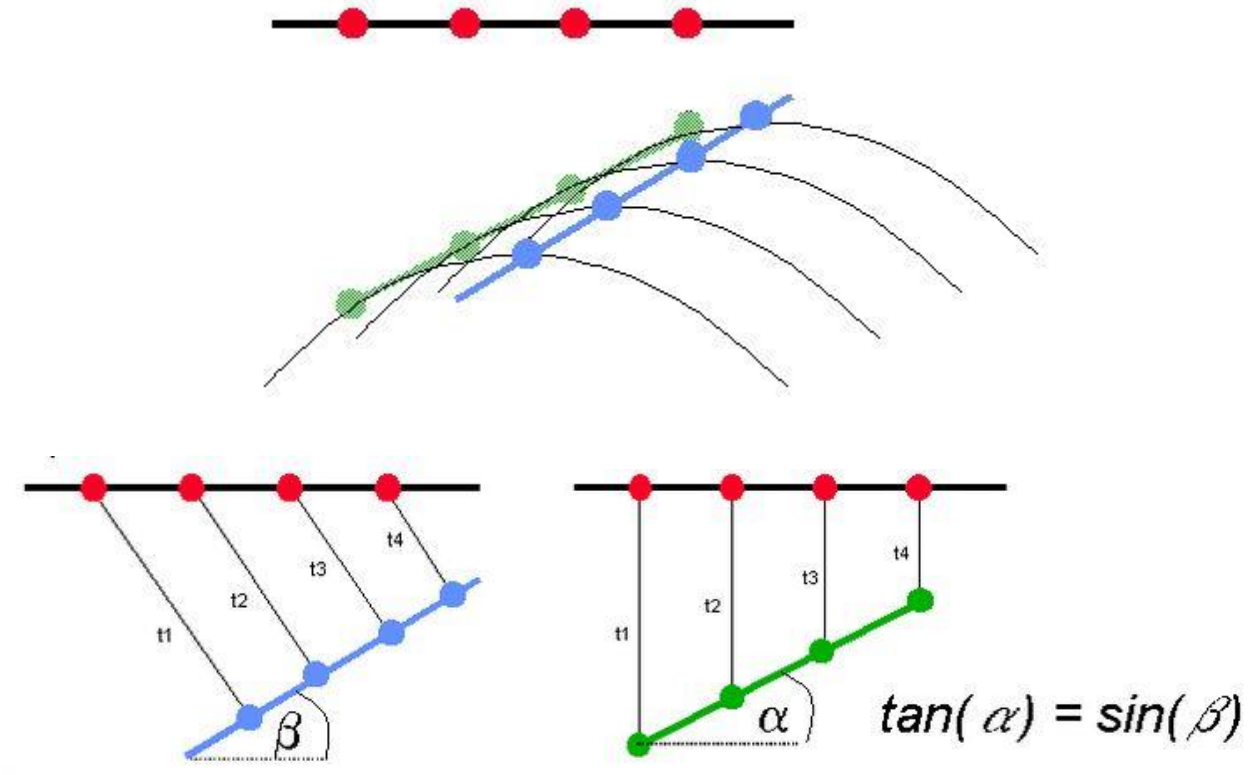

Fig.4 Migration of a line

2. Soil surface

The roughness of any scattering surfaces is not an intrinsic property of that surface but depends on the properties of a wave being transmitted. Both, the frequency and the local angle of incidence of the transmitted wave, determine how rough or smooth any surface appears to be.

In the near field of the propagating EM wave, the surface appears rougher than in the far field, which can be compared with the reflection of the sunset over the sea.

In case of an ideal smooth surface the characteristics of the reflection can be described by the well-known Fresnel Reflectivity.

$$\Gamma_h(\theta) = \frac{\mu\cos\theta - \sqrt{\mu\varepsilon - \sin^2\theta}}{\mu\cos\theta + \sqrt{\mu\varepsilon - \sin^2\theta}} \qquad \Gamma_v(\theta) = \frac{\varepsilon\cos\theta - \sqrt{\mu\varepsilon - \sin^2\theta}}{\varepsilon\cos\theta + \sqrt{\mu\varepsilon - \sin^2\theta}}$$

Where Γ_h and Γ_v are the horizontal and vertical polarization of the EM wave and μ is always for non-ferromagnetic media, as natural surfaces, equal to one.

In the natural environment the surface condition varies from medium to rough. The backscattered EM wave on a surface consists of two components, a reflected or coherent and a scattered or incoherent one.

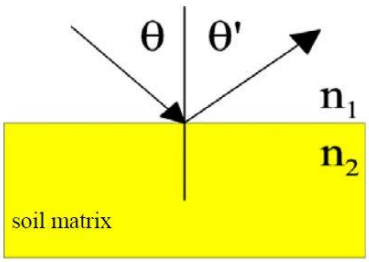

Fig.5 Fresnel reflection scheme

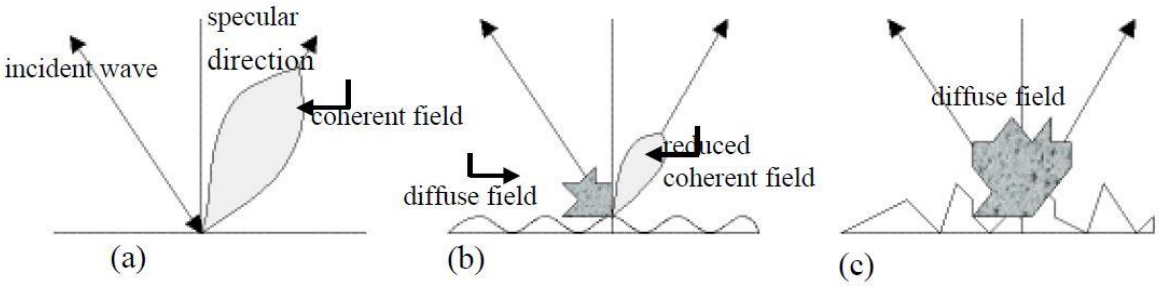

Fig.6 Roughness components in a (a) smooth, (b) rough and (c) very rough surfaces.

The coherent component reacts as a specular reflection on a smooth surface, and the incoherent component is a diffuse scatterer and distributes the scattering power in all directions. As the surface becomes rougher, the coherent component becomes negligible and the incoherent component consists of only diffuse scattering.

Defining a surface from an electromagnetic point of view as smooth or rough, is somewhat arbitrary. Nevertheless two main criteria can be found to define a smooth surface, the Rayleigh and the Frauenhofer criterion. Considering a plane monochromatic wave transmitted at some angle onto a rough surface, it is a simple matter to calculate the phase difference between two rays scattered from separate points on the surface:

$$\Delta\phi = 2h\frac{2\pi}{\lambda}\cos\theta$$

Where h is the standard deviation of the roughness height regarding to a reference height and the local incident angle.

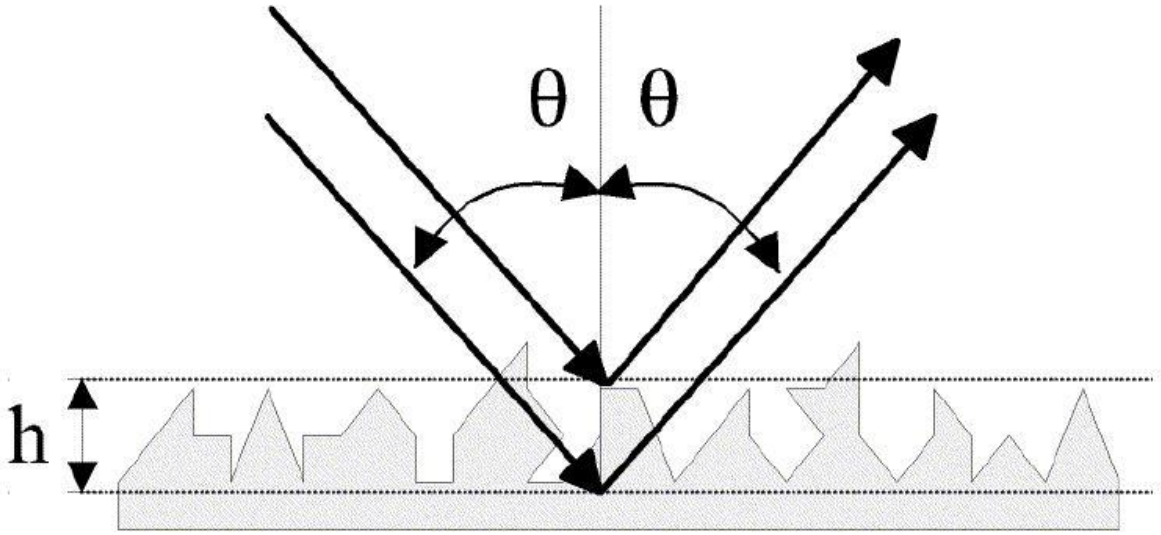

Fig.7 Phase difference between two parallel waves scattered from two points on a rough surface

The Rayleigh criterion states that if the phase difference Δϕ between two reflected waves is less than π / 2 radians, than the surface may be considered as smooth, and is defined by

$$h < \frac{\lambda}{8\cos\theta}$$

The usage of a more stringent criterion, which is adapted to the EM wave region, is called Frauenhofer criterion. This criterion considers a surface as smooth, if the phase difference is Δϕ< π / 8 . [1]

$$h < \frac{\lambda}{32\cos\theta}$$

3. Wave propagation in lossy dielectric

A lossy dielectric is a medium in which an EM wave loses power as it propagates due to poor conduction.

In other words, a lossy dielectric is a partially conducting medium (imperfect dielectric or imperfect conductor) with σ≠ 0, as distinct from a lossless dielectric (perfect or good dielectric) in which σ = 0.

Consider a linear, isotropic, homogeneous, lossy dielectric medium that is charge free

($p_v = 0$). Assuming and suppressing the time factor $e^{j\omega t}$, Maxwell's equations become

$$\nabla \cdot \mathbf{E}_s = 0$$

$$\nabla \cdot \mathbf{H}_s = 0$$

$$\nabla \times \mathbf{E}_s = -j\omega\mu\mathbf{H}_s$$

$$\nabla \times \mathbf{H}_s = (\sigma + j\omega\varepsilon)\mathbf{E}_s$$

Taking the curl of both sides of the third equation and simplifying gives

$$\nabla^2\mathbf{E}_s - \gamma^2\mathbf{E}_s = 0$$

Where

$$\gamma^2 = j\omega\mu(\sigma + j\omega\varepsilon)$$

γ is called the propagation constant (in per meter) of the medium.

If we assume that the wave propagates along +az and that Es has only an x-component, and the field must be finite at infinity we obtain the solution of the differential equation

$$E_{xs}(z) = E_o e^{-\gamma z}$$

Since γ is a complex quantity

$$\gamma = \alpha + j\beta$$

We can obtain α and β such as

$$\alpha = \omega\sqrt{\frac{\mu\varepsilon}{2}\left[\sqrt{1+\left[\frac{\sigma}{\omega\varepsilon}\right]^2}-1\right]}$$

$$\beta = \omega\sqrt{\frac{\mu\varepsilon}{2}\left[\sqrt{1+\left[\frac{\sigma}{\omega\varepsilon}\right]^2}+1\right]}$$

Where α is the attenuation factor and β is the phase constant and the ratio σ/ωε is the loss tangent.

Plane waves of constant phase will propagate with a velocity

$$v = \frac{\omega}{\beta} = c\left[\frac{\epsilon'}{2}\left[\sqrt{1+\left[\frac{\epsilon''}{\epsilon'}\right]^2}+1\right]\right]^{-1/2}$$

Power attenuation expressed in decibels per meter can then be written as

$$PL = -8.6859\,\frac{\omega}{c}\left[\frac{\epsilon'}{2}\left[\sqrt{1+\left[\frac{\epsilon''}{\epsilon'}\right]^2}-1\right]\right]^{1/2}$$

4. Soil texture

Researches have shown that the soil dielectric constant is dependent on soil texture, along with it has been proved that change in dielectric constant with moisture shows its dependency on soil texture. [2]

Name of soil separates	Diameter limits (mm)
Sand	2–0.05
Silt	0.05–0.002
Clay	Less than 0.002

Soils are classified according to their particle size texture. Water in a soil medium consists of two components, adsorbed and free. The adsorbed molecules are held tightly to the soil particles in the form of thin layers a few molecules thick, whereas the free molecules usually occupy the empty spaces between the soil particles. The size of a soil particle is of major importance so far as the ratio of the number of free water molecules to adsorbed molecules is concerned. Thus, for a soil medium, this ratio depends on the particle size distribution and the total water content.

Because of its limited mobility, adsorbed water may have a much smaller permittivity than that of free water by as much as a factor of 10. Hence, the microwave scattering properties of a soil medium may in turn depend on its soil texture in low moisture soil. [3]

5. Soil dielectric properties

The permittivity of soil is strongly dependent on its moisture content. Hence, corresponding to a given soil moisture depth profile, a permittivity profile exists which influences the interaction of an electromagnetic wave at the air soil interface as well as the wave propagation properties inside the soil medium. [3]

The figure below shows the different mechanisms that affect the dielectric constant in most materials.

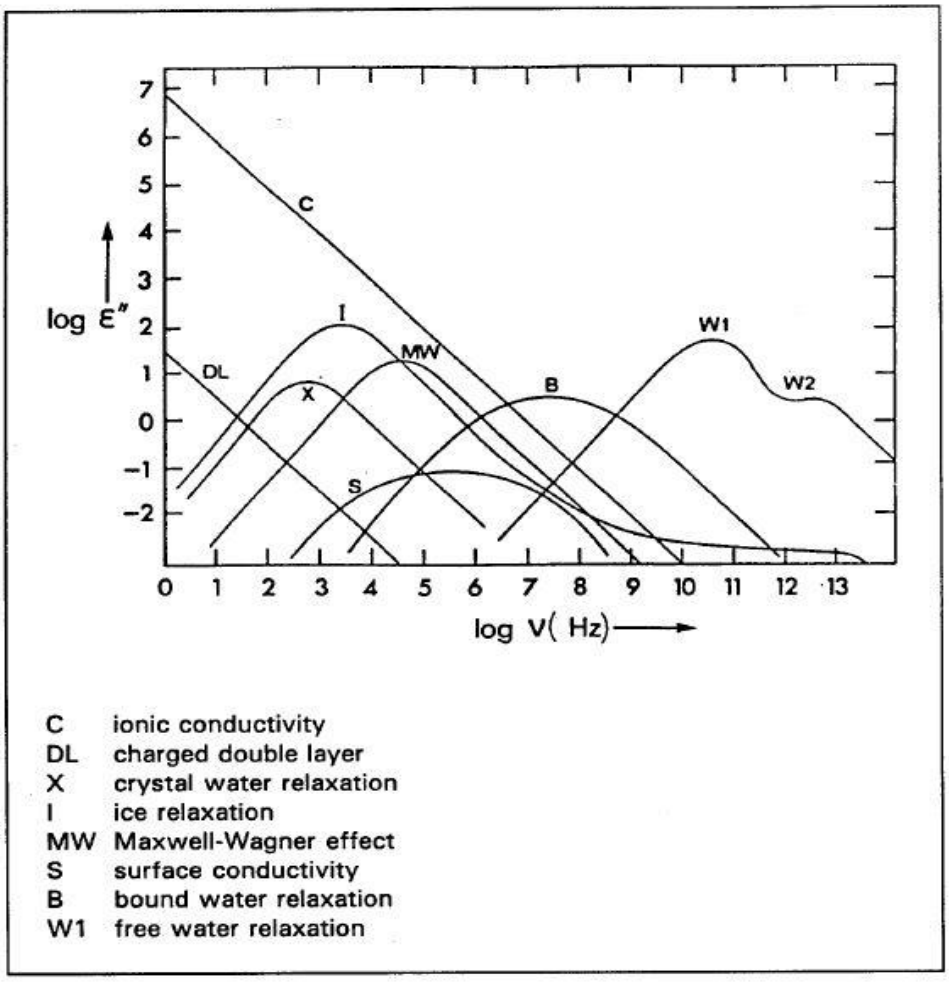

Fig.8 Dielectric loss mechanisms for heterogeneous moist materials

In this study we will focus on the region around 2Ghz.The dominant mechanism in our region of interest is the free water relaxation, and it involves free water molecules.

Individual water molecules can be considered to be electric dipoles. In the presence of an oscillating electric field, the dipoles will try to align themselves with the field.

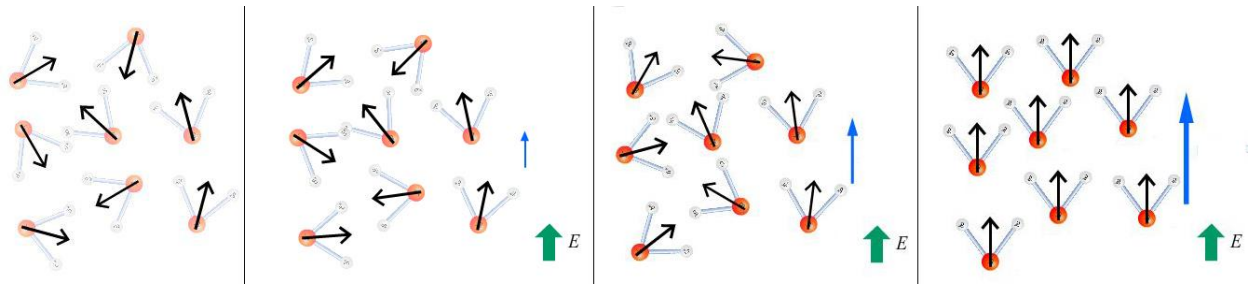

Fig.9 Free water relaxation mechanism

As one increases the frequency of the oscillating field, the dipoles are forced to rotate more and more quickly. At some frequency, the dipoles will start to lag behind the forcing field due to rotational inertia and viscosity. At this point, the permittivity of the substance starts to decrease, and the imaginary part of the dielectric constant starts to increase to reflect the increasing lag between the electric field and the orientation of the water dipole. As the frequency of the field further increases, the dipoles get to the point where they do not respond to the field at all, resulting in minimum values for both the real and imaginary parts of the complex dielectric constant. This behavior is referred to as anomalous. It is also referred to as a relaxation phenomenon with regard to the measure of the dipole's ability to return to its equilibrium position, or "relax," after the removal of an electric field. [4]

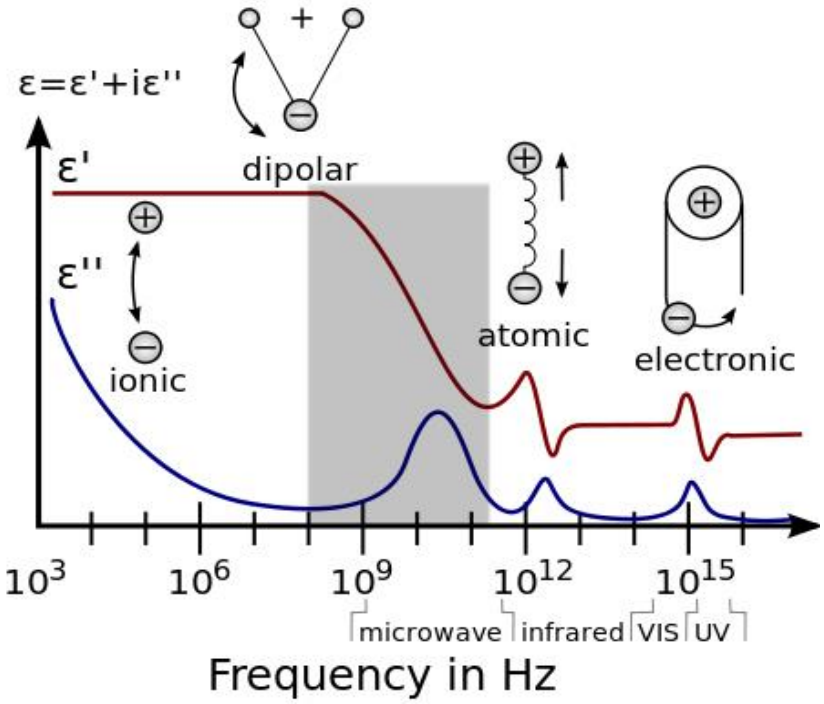

Fig.10 Dielectric response depending on frequency

6. Scattering theory

Snell's law accurately determines the propagation directions of the reflected and transmitted waves at the boundary of two materials with different refractive indexes. However, Snell's law gives no information about the amplitude of the two waves, but it can be determined by using Maxwell's equations with the boundary conditions associated with these equations.

TE polarization

For TE polarization (also called s polarization), the electric field is perpendicular to the plane of incidence, as shown in the figure below.

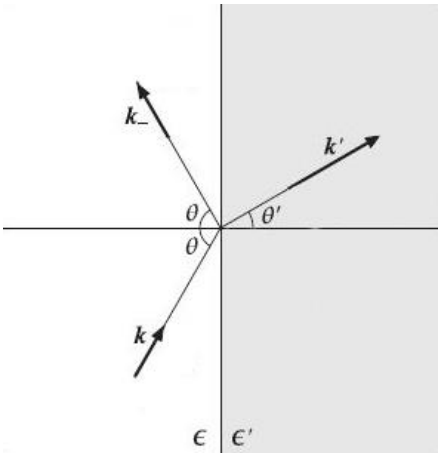

Fig.11 Snell's law of refraction

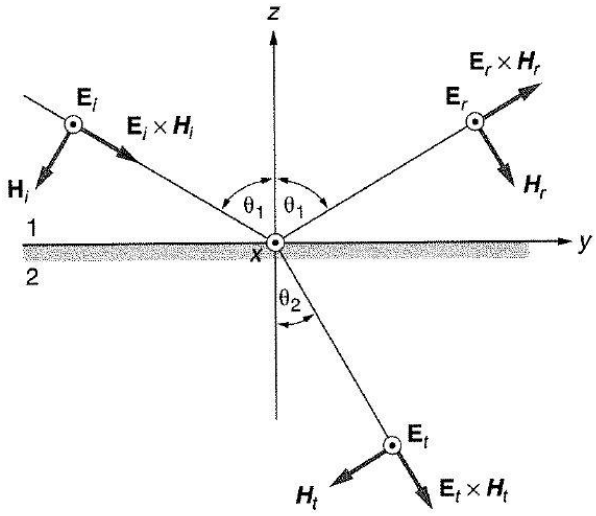

Fig.12 TE incidence

H field on the two sides of the interface is equal. This results in the following two equations

$$E_{1i} + E_{1r} = E_2 \qquad (H_{1i} - H_{1r})\cos\theta_1 = H_2 \cos\theta_2$$

Since $H_{1i}=E_{1i}/\eta_1$, $H_{1r}=E_{1r}/\eta_1$ and $H_2=E_2/\eta_2$, we have two linear equations in two unknowns E_{1r} and E_2, solving these equations we obtain

TM polarization

For TM polarization (also called p polarization) the electric field is parallel to the plane of incidence

$$\rho_n = \left(\frac{E_{1r}}{E_{1i}}\right)_n = \frac{\eta_2 \cos\theta_1 - \eta_1 \cos\theta_2}{\eta_2 \cos\theta_1 + \eta_1 \cos\theta_2},$$

$$\tau_n = \left(\frac{E_2}{E_{1i}}\right)_n = \frac{2\eta_2 \cos\theta_1}{\eta_2 \cos\theta_1 + \eta_1 \cos\theta_2}.$$

The boundary conditions in this case

$$(E_{1i} - E_{1r})\cos\theta_1 = E_2\cos\theta_2$$

$$H_{1i} + H_{1r} = H_2.$$

Expressing magnetic field intensities as E/η, we again obtain two linear equations with unknowns E_{1r} and E_2. The solution of these equations is

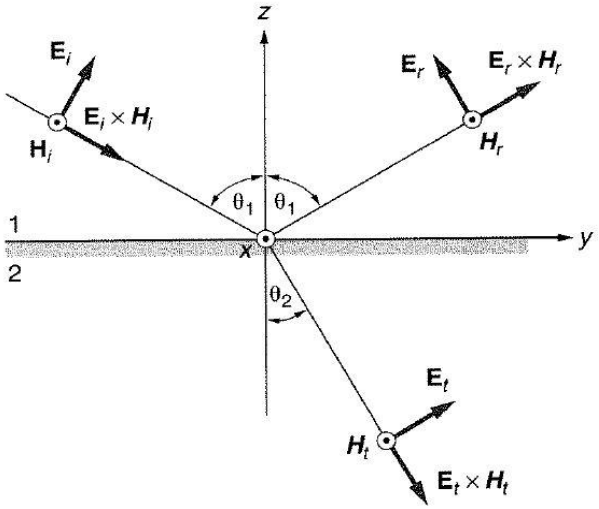

Fig.13 TM incidence

$$\rho_p = \left(\frac{E_{1r}}{E_{1i}}\right)_p = \frac{\eta_1\cos\theta_1 - \eta_2\cos\theta_2}{\eta_1\cos\theta_1 + \eta_2\cos\theta_2},$$

$$\tau_p = \left(\frac{E_2}{E_{1i}}\right)_p = \frac{2\eta_2\cos\theta_1}{\eta_1\cos\theta_1 + \eta_2\cos\theta_2}.$$

Critical angle

As the incident angle θ varies over 0 ≤ θ ≤ 90o, the angle of refraction θ' will have a corresponding range of variation. It can be determined by solving for θ' from Snel's law, nsinθ = n' sinθ'

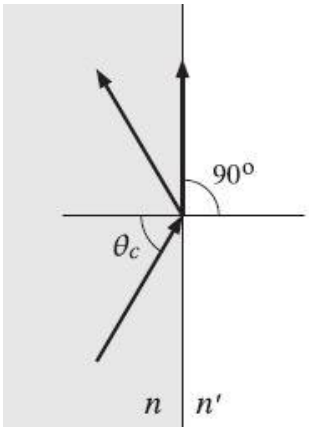

If n < n' then sinθ' = (n/n')*sinθ < sinθ, or θ' < θ. Thus, if the incident wave is from a lighter to a denser medium, the refracted angle is always smaller than the incident angle. The maximum value of θ', denoted here by θ'_c, is obtained when θ has its maximum, θ = 90°.

Fig.14 Critical angle

$$\sin\theta'_c = \frac{n}{n'}$$

Brewster angle

The Brewster angle is that angle of incidence at which the TM Fresnel reflection coefficient vanishes, $\rho_{TM} = 0$. The TE coefficient ρ_{TE} cannot vanish for any angle θ, for non-magnetic materials.

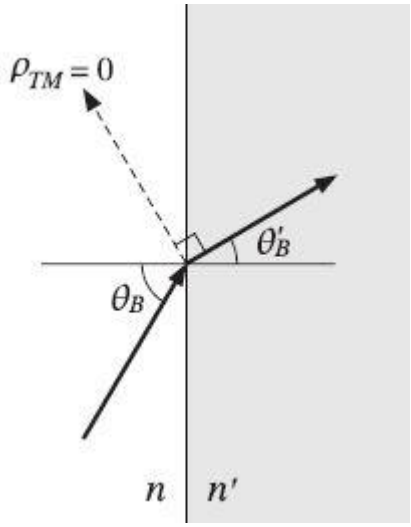

Fig.15 Brewster angle

The Brewster angle is also called the polarizing angle because if a mixture of TM and TE waves are incident on a dielectric interface at that angle, only the TE or perpendicularly polarized waves will be reflected. This is not necessarily a good method of generating polarized waves because even though ρ_{TE} is non-zero, it may be too small to provide a useful amount of reflected power.

The Brewster angle θ_B is determined by the condition, $\rho_{TM} = 0$, we obtain the following relation

$$\tan\theta_B = \frac{n'}{n}$$

7. Material heating

When dealing with moist materials such as soil, the dominant loss mechanism is dipole heating due to the presence of water. On the other hand, there is virtually no water in a non-conducting insulator (von Hippel, R., *Dielectric Materials and Applications*, M.I.T. Press, aug. 1966.) such as nylon or other synthetic substances. In addition, the Maxwell-

Wagner type effects (Neelakanta, P.S., *Handbook of Electromagnetic Materials*, CRC Press, Jan. 1995.) play no part in the heating process for a homogeneous material with few impurities. Hence, the only heating mechanism is a result of the dipolar nature of the material itself and, in general, plastics heat at a much slower rate than the surrounding soil.

The heating rate in plastics can be related to the dielectric constant by

$$\Delta T = P \Delta t / (m c_p)$$

Where

$$P = \omega \varepsilon'' E^2$$

A typical heating rate can be calculated by

$$\Delta T = \omega \varepsilon'' E^2 \Delta t / (m c_p)$$

$$\Delta T = (E^2 \Delta t / \upsilon) \omega \varepsilon'' / (\rho c_p)$$

where v is the sample volume. By substituting the values of ε", c_p and ρ for generic soil and Plexiglas (which, for a plastic, is a relatively strong microwave absorber) the relative heating rates can be calculated as

$$\frac{\Delta T_{soil}}{\Delta T_{plexiglas}} = \frac{\left\{ \frac{\varepsilon''_{soil}}{(\rho_{soil} c_{p(soil)})} \right\}}{\left\{ \frac{\varepsilon''_{Plexiglas}}{(\rho_{Plexiglas} c_{p(Plexiglas)})} \right\}}$$

Let's take ε"= 0.16 for water and 0.0148 for Plexiglas, this gives us a ratio of 9.

The result indicates that the heating rate for soil is, in general, significantly larger than for plastics. Therefore, the soil around the mine or mine surrogate will heat at a faster rate than the target itself.

One factor may help alleviate the above problem. The dielectric constant of a material can be strongly influenced by temperature. In microwave heating applications, thermal runaway is defined as an uncontrolled rise of the temperature due to the positive slope on the ε" versus temperature curve. This causes further absorption and, in turn, additional heating. This cycle

repeats to further increase the temperature. This effect may be present in some mine bodies or explosives.(Huang, H.F., Temperature Control in a Microwave Resonant Cavity for Rapid Heating of Nylon Monofilament, *Journal of Microwave Power*, 11(4), pg. 305-313, 1975.)

CHAPTER II: CONTRIBUTION AND RESULTS

1. Frequency of interest

Taking into consideration that the commercial microwaves heating devices that are available operate on a 2.45 GHz frequency, and it's suitable for water heating. And the patch antennas we are capable to manufacture have the best gain at 1.6GHz, and that frequency corresponds to a wavelength around 18.75 cm which is good in our case working with objects that have dimensions from 10 to 20 cm (>λ/10 and <10λ) and gives good resolution since we are interested in discontinuities in the landmine body. We are going to work with 1.6 GHz in the GPR simulation where we would be interested in the scattered wave, and 2.45 GHz in the simulations where we would be interested in the transmitted power.

2. Soil types

First of all before beginning with simulations we have to choose models for the soil we are working on, describing it exactly as seen in the microwave scale.

Works are done before by the US Army corps of engineers 1995, to extract the dielectric properties of different soil types on different frequencies and at different temperatures and different moisture content.

We chose these types from a list of 12 soil types

Sample	Description	Sand percentage	Silt percentage	Clay percentage
A	Sand, Light Grey	98	2	-
B	Silty Sand, Reddish Brown	77	9	14
C	Clayey Silt, Brown	-	93	7
D	Sand, White	100	-	-

Table.1 Soil types

We extracted the dielectric properties for these soils on our frequency of interest (1.5-2.5 GHz) with different moisture contents.

Sample	Moisture percentage	Real permittivity	Loss tangent
A	0.53%	3	0.1
	16.7%	9	0.07
	36.6%	21	0.1
B	3.2%	2.7	0.07
	13.2%	5.2	0.07
	39.4%	22	0.09
C	6%	3	0.11
	12.5%	7.5	0.2
	42.8%	28	0.2
D	0.4%	2.6	0.05
	13.3%	8	0.08
	33.8%	21	0.11

Table.2 Dielectric properties of different soils used in simulations

3. Models test

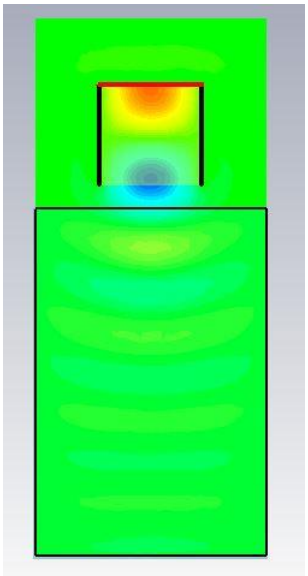

Theoretically, the attenuation factor depends on the dielectric constant and the loss tangent with the following relation

$$\alpha = \omega\sqrt{\frac{\mu\varepsilon}{2}\left[\sqrt{1+\left[\frac{\sigma}{\omega\varepsilon}\right]^2}-1\right]}$$

To verify the validity of the soil model we did a number of simulations on each soil type, using the CST Microwave Studio and probed the electric field along the wave trajectory, and then plotted the power attenuation with respect to depth.

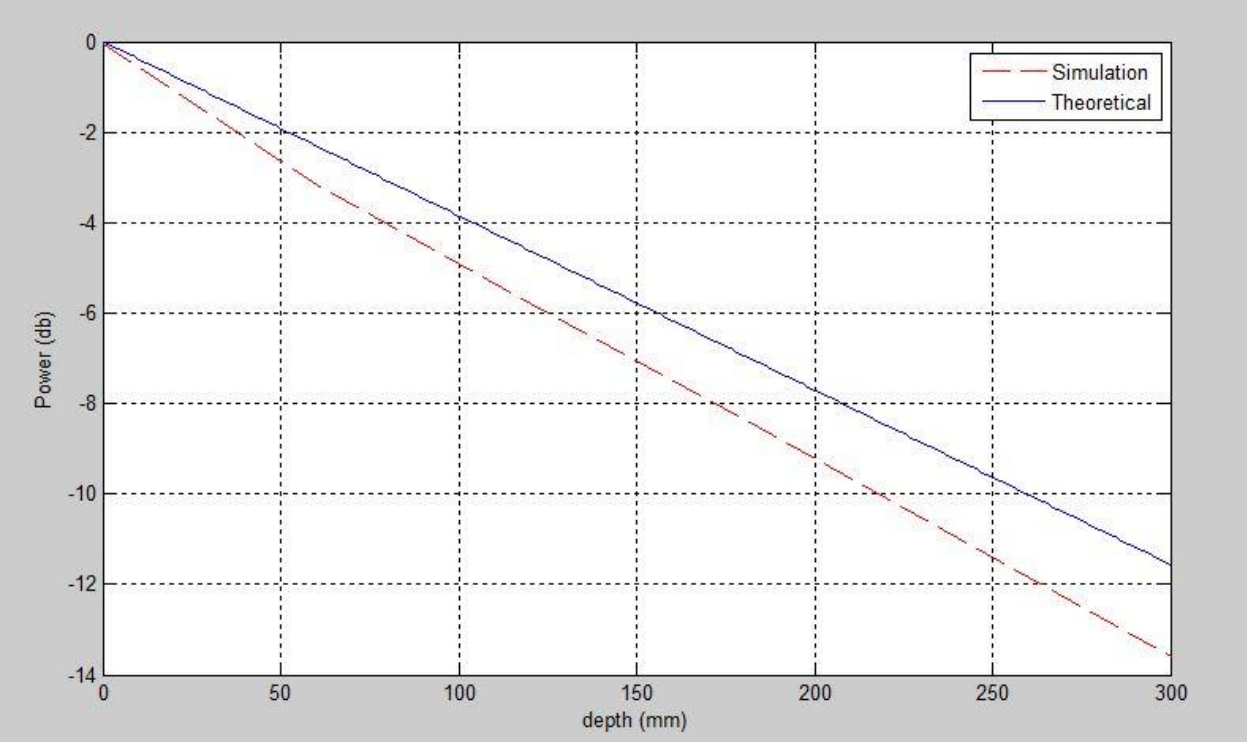

Fig.16 Power attenuation respect to depth (theoretical and simulation results)

The plot above shows the line calculated theoretically describing the power attenuation with respect to the depth, and the results collected from the simulation at 2.45 GHz in the soil A at 0.53% moisture content.The two lines are relatively close, but there is still a 2 db difference.

We did the measurements for the rest of soil types

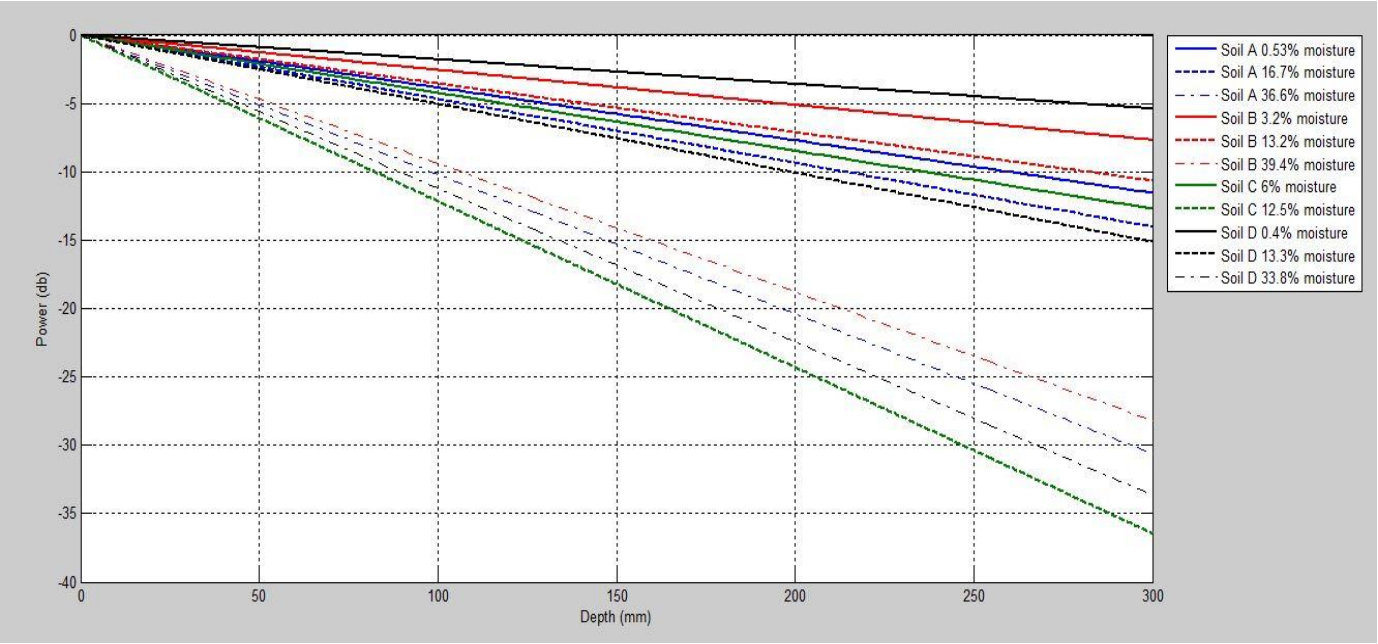

Fig.17 Theoretical results

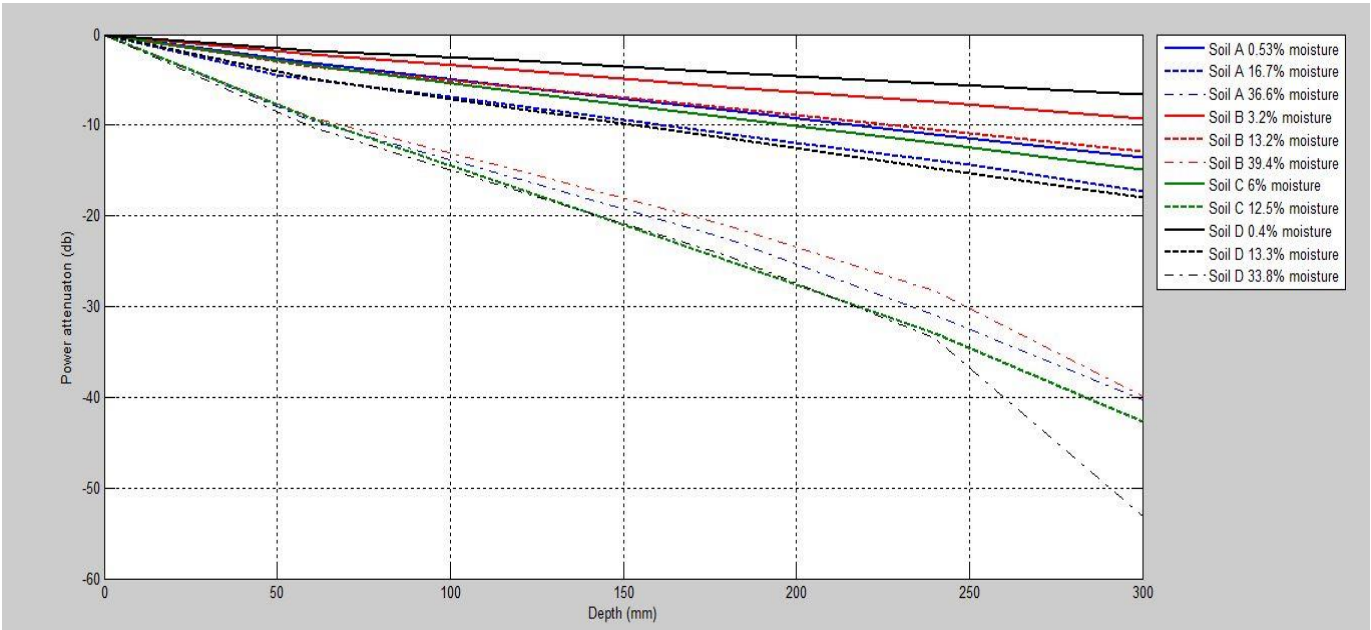

Fig.18 Simulation results

The results shows a similarity between the theoretical and measured values for the power attenuation, which allows us to work with these models in the later simulations.

We can see also that the power attenuation take a similar decrease with different soil types and changes in the same way with the moisture increase. Knowing this we can avoid doing a lot of useless simulations.

And practically, the demining process would rarely or even never take action in high moisture soils (above 20%) due to the difficulties in setting up and moving the equipments. Therefore, working with real soil, we could estimate average dielectric properties for the soil, to use in compensation and to estimate an average exposure time, which we'll be discussing later in this report.

4. Incidence angle responce

The propagation of EM waves between two mediums with different dielectric constants depends on the incidence angle and the incidence mode, which have a huge impact on the reflection and transmission coefficients as we can see in the equations.

TE:

$$\rho_n = \left(\frac{E_{1r}}{E_{1i}}\right)_n = \frac{\eta_2 \cos\theta_1 - \eta_1 \cos\theta_2}{\eta_2 \cos\theta_1 + \eta_1 \cos\theta_2},$$

$$\tau_n = \left(\frac{E_2}{E_{1i}}\right)_n = \frac{2\eta_2 \cos\theta_1}{\eta_2 \cos\theta_1 + \eta_1 \cos\theta_2}.$$

TM:

$$\rho_p = \left(\frac{E_{1r}}{E_{1i}}\right)_p = \frac{\eta_1 \cos\theta_1 - \eta_2 \cos\theta_2}{\eta_1 \cos\theta_1 + \eta_2 \cos\theta_2},$$

$$\tau_p = \left(\frac{E_2}{E_{1i}}\right)_p = \frac{2\eta_2 \cos\theta_1}{\eta_1 \cos\theta_1 + \eta_2 \cos\theta_2}.$$

We are more interested here in the transmission, but knowing the existence of special angles like Brewster angle we can expect to find an angle with better transmission coefficient than the normal incidence.

We made simulations on the soil A with 0.5% moisture content, and we recorded the power attenuation at 10 cm depth for incidence angle varying from 0 to 60 degree (0 degree being he normal incidence).

We got the following graphs for TE and TM modes respectively.

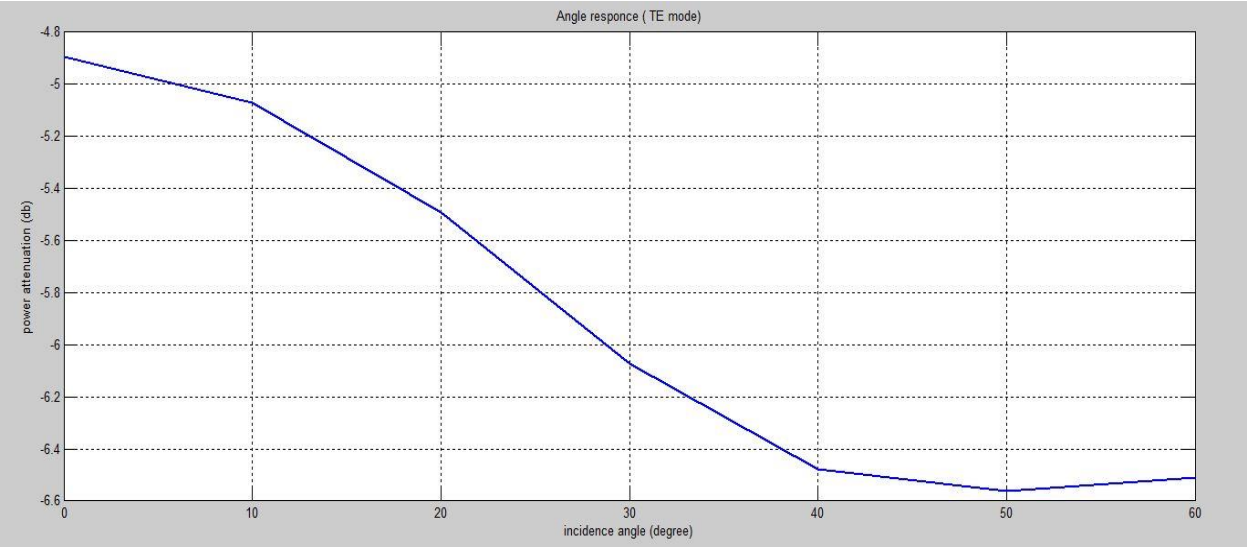

Fig.19 Angle response TE mode

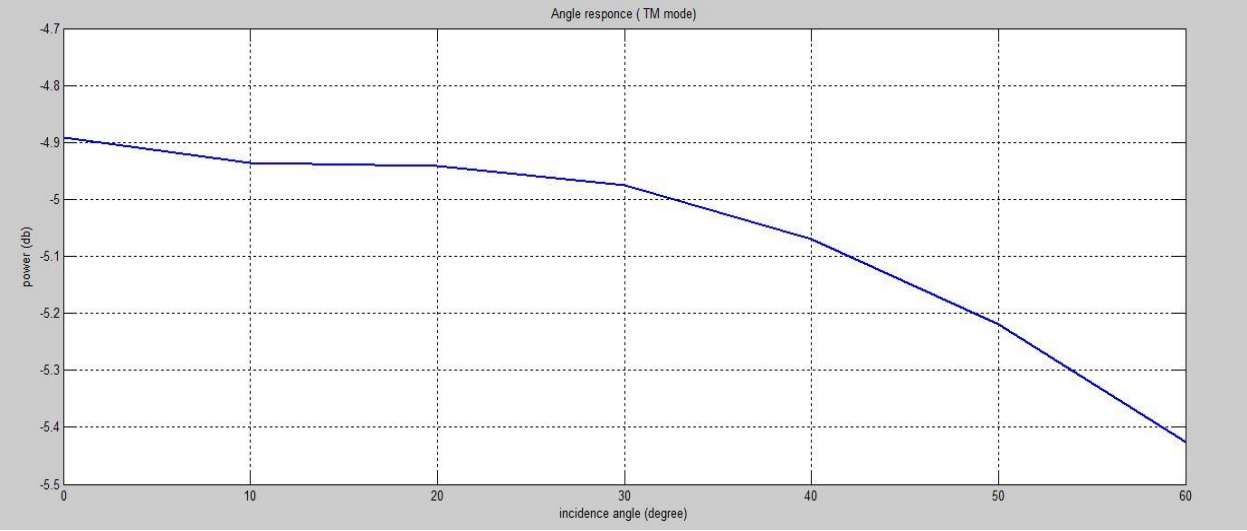

Fig.20 Angle response TM mode

These results clearly shows us that the better transmission is for the normal incidence in both TE and TM modes, and the Brewster angle (with 0 reflection coefficient) doesn't imply a total transmission but either a surface wave or dissipated wave.

These simulations provide us with useful information to estimate the amount of power and exposure time needed to reach a specific temperature in a specific depth (The temperature needed to work the detonator is still unknown, waiting to be provided by the military specialists), these values can be calculated from the equation that shows he relation between the time, power and temperature provided previously in this report.

5. Used antennas

For the GPR simulation we choose a microstrip patch antenna designed by Dr.Mohammed Al-Husseini [5], for the transmitter and receiver. The benefits of that antenna are the ease of manufacturing and the cheap cost, as well as a decent gain in the frequency of interest (2.8 db).

The simulation was made to test the insertion loss of the antenna, and we got results similar to the paper.

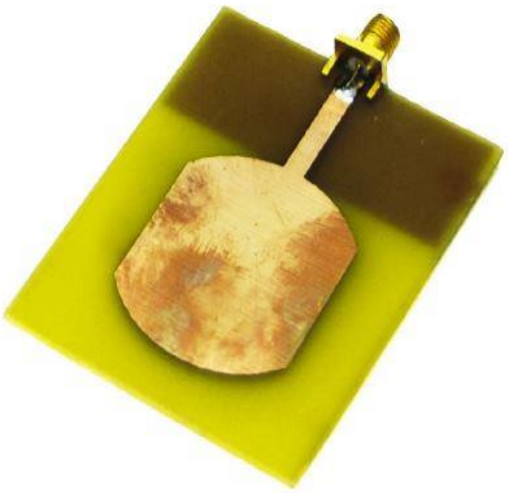

Fig.21 fabricated antenna

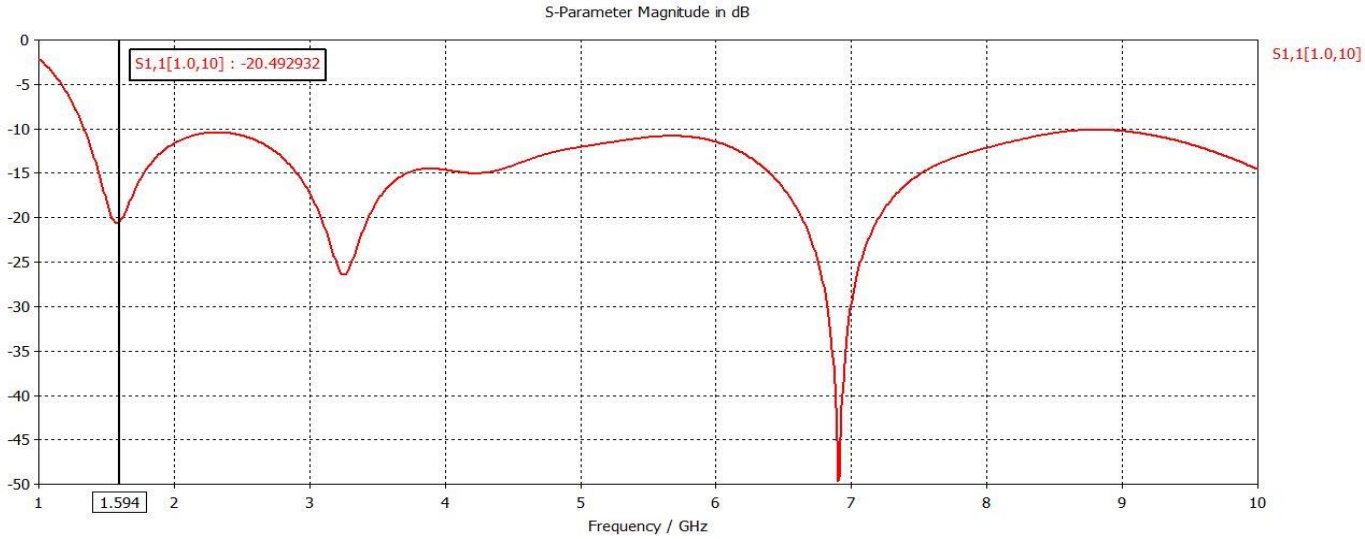

Fig.22 Return Loss for the patch antenna

To set up the Tx and Rx system we have to take into consideration the coupling between the two antennas. We got acceptable return loss (-17.7 db) and insertion loss (-14 db) after separating the antennas by 93.75 mm distance (5 lambda, from center to center).

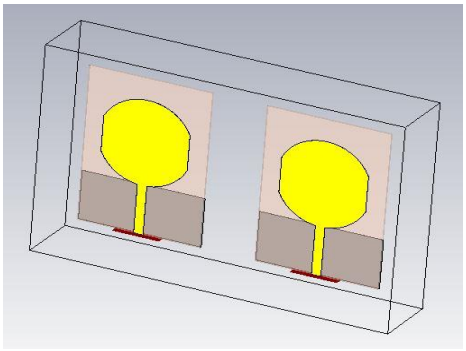

Fig.23 Antennas used in GPR simulation

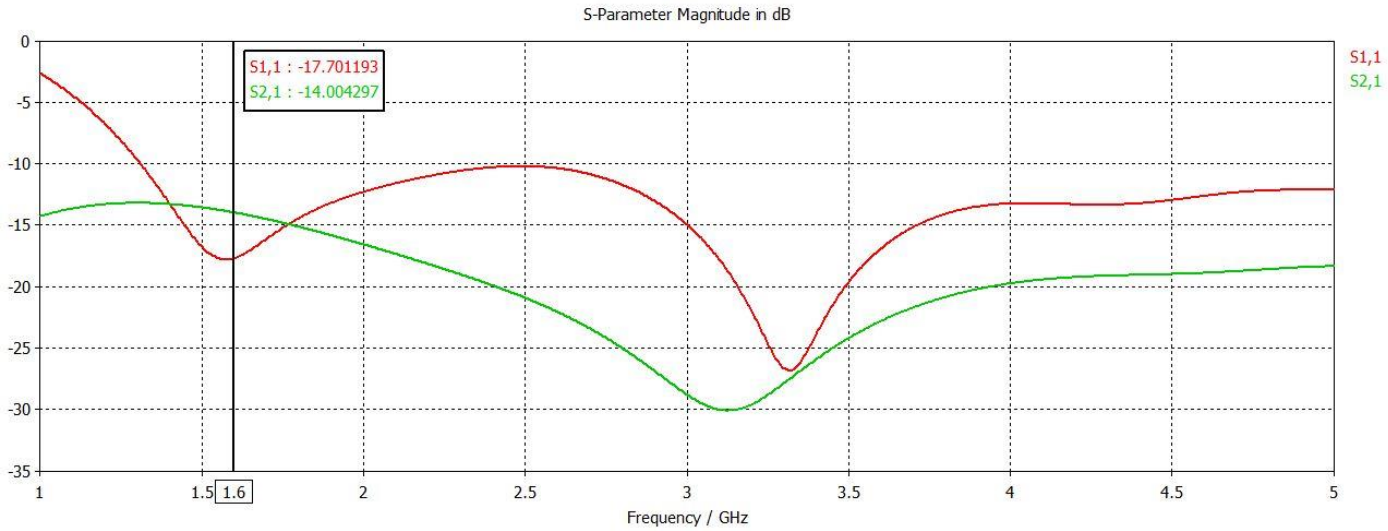

Fig.24 Return loss and insertion loss after coupling the two antennas

6. Environment setup

To model our soil test bed for the simulation, we use a homogeneous dielectric layer with the dimensions needed and corresponding dielectric properties, surrounded by absorber materials (ECCOSORB) to prevent reflection in directions considered to be infinite in real soil, but happens to be an interface between soil and air in the simulation due to the specified dimensions of the test bed that are bounded by computational limits.

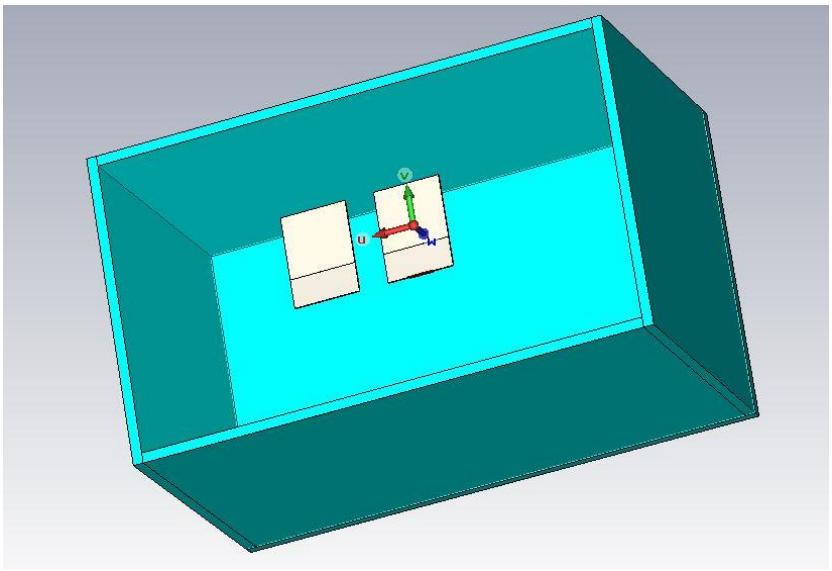

Fig.25 Simulation environment

We chose the dimensions considering that the depth of interest in the practical case will be no more than 30 cm underground.

7. GPR simulation

After setting up the GPR and soil model (The soil used in all the GPR simulations is the soil A with 0.53% moisture content), the antennas were positioned in the center and 1 cm above the soil surface, and the scanning trajectory have to be defined. But due to the limitation in the soil dimensions, it is more suitable to move the target instead along the U axis.

The excitation signal used is a Gaussian pulse centered on 1.6 GHz.it is sent through the first port, and the received data is collected through the second port.

The solver we are going to use is a transient solver, because the essential data we are basing our work on lies within the discontinuities in the received signal, and the desired signal at the receiver should be a time signal to extract information from such as target depth.

Knowing that the RTT for 30 cm depth is 5.2 ns, we set the simulation time to 10 ns, in order to collect all the directly and indirectly reflected signals.

7.1. Cylindrical target

The first and simplest target we began simulation with is a cylindrical target. The scan being two dimensional (antennas trajectory in U axis, and the time thus soil depth in W axis) we put the cylinder axis aligned with the V axis so the target looks like a point in the resulting image.
First simulation was ran, and the collected signal in each iteration has the following form

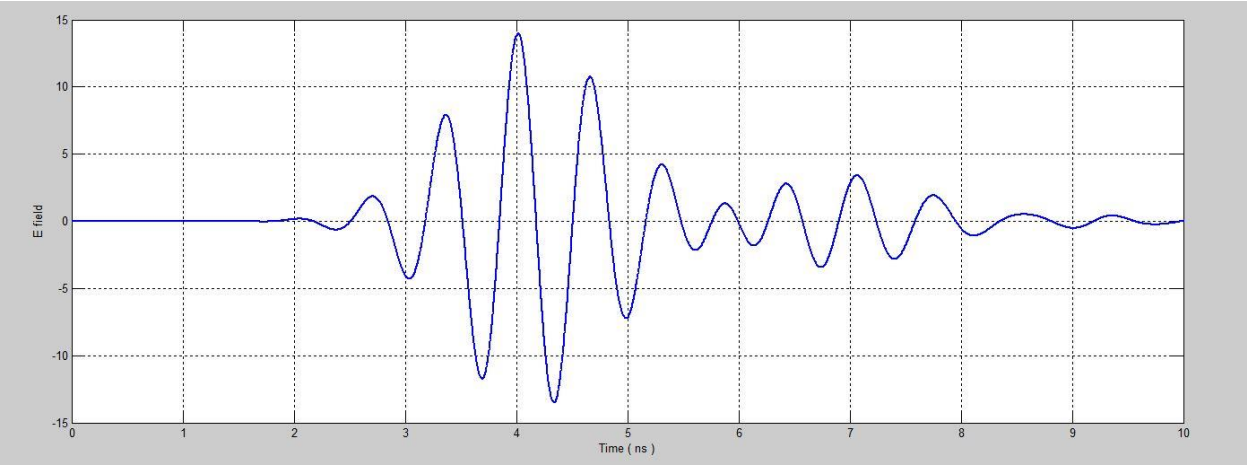

Fig.26 E field record collected at the receiver in one iteration

These signals are gathered and plotted in MATLAB to give us the following image

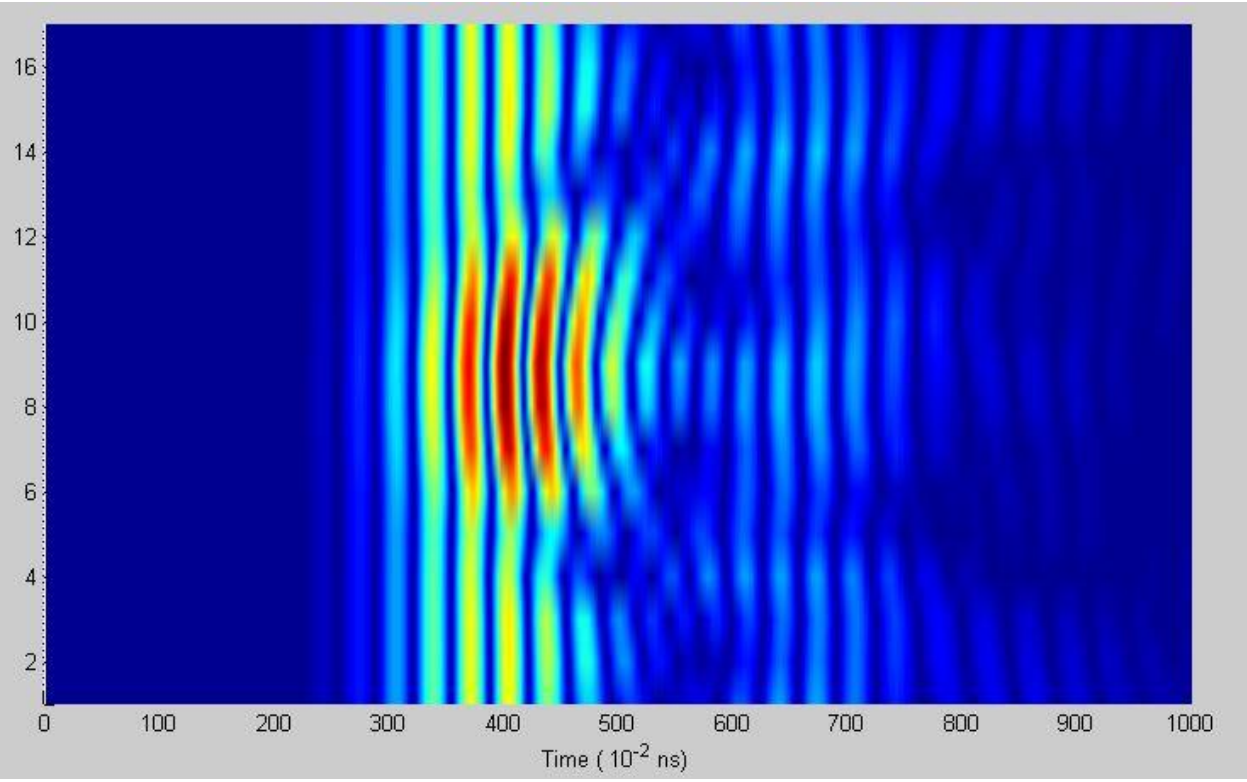

Fig.27 GPR image for cylindrical target

This image contains scattered signals from the target and the soil surface in interference with each other. To extract the signal reflected from the target alone we have to do a soil compensation and that would be by subtracting the signal reflected from the empty soil.

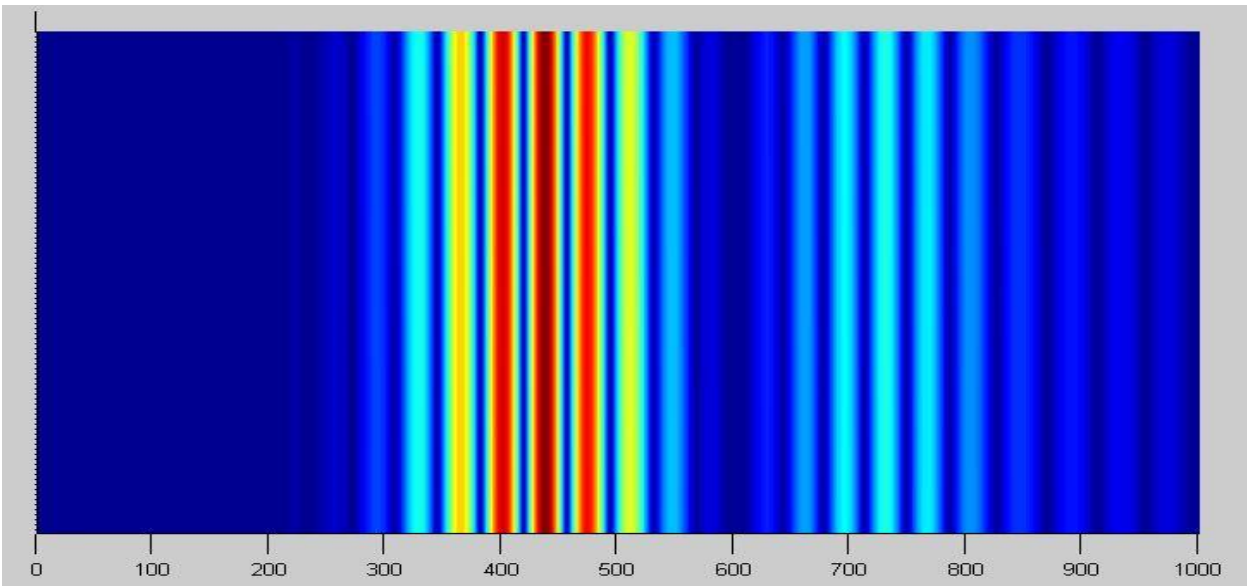

Fig.28 GPR image for empty soil (background image)

After subtracting the soil image we get the following image

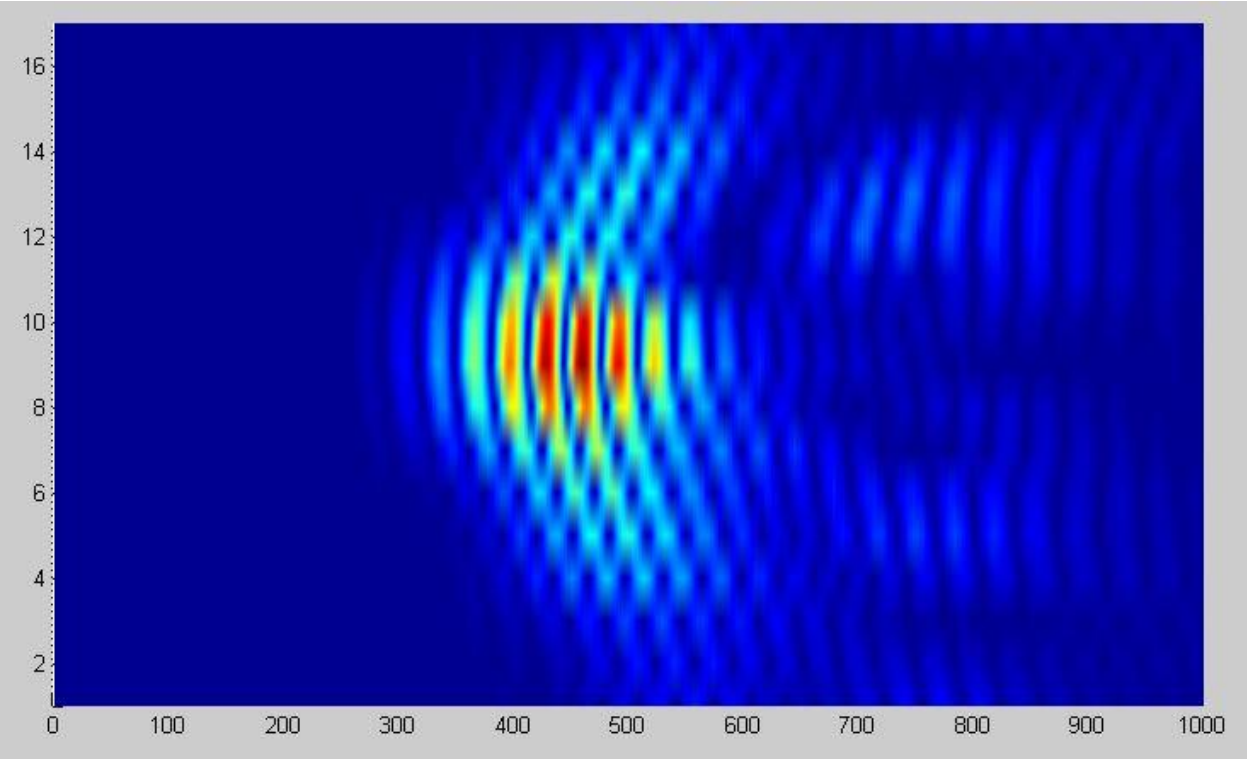

Fig.29 GPR image of cylindrical target after compensation

The hyperbolic shape is clearly observed due to the migration. And the real depth of the target is slightly changed due to this. Therefore to extract the useful information corresponding algorithms needs to be applied.

Any further interpretation of the results would be done by the recognition system.

Variations of this work have been done, to observe the influence of different parameters on the Image of the target.

Depth influence

This simulation was done for respectively 5, 10, 15, 20 cm depths to compare between the images constructed.

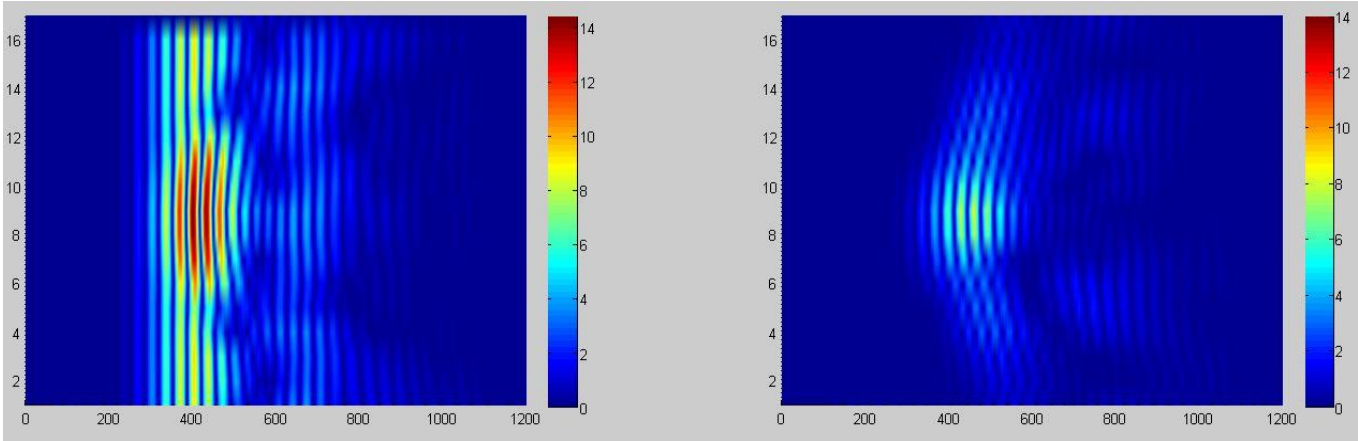

Fig.30 GPR image for the cylinder at 50 mm depth

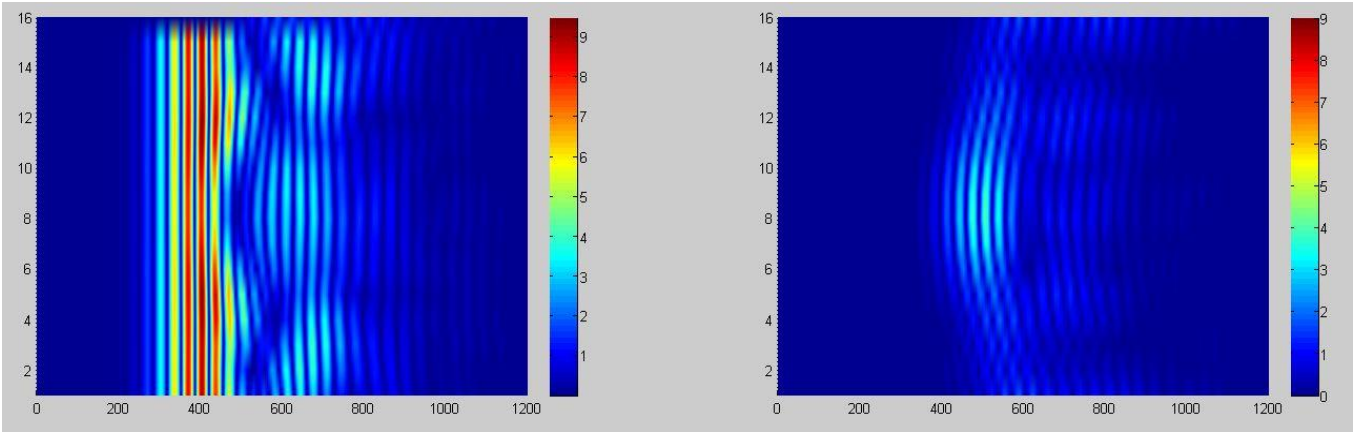

Fig.31 GPR image for the cylinder at 100 mm depth

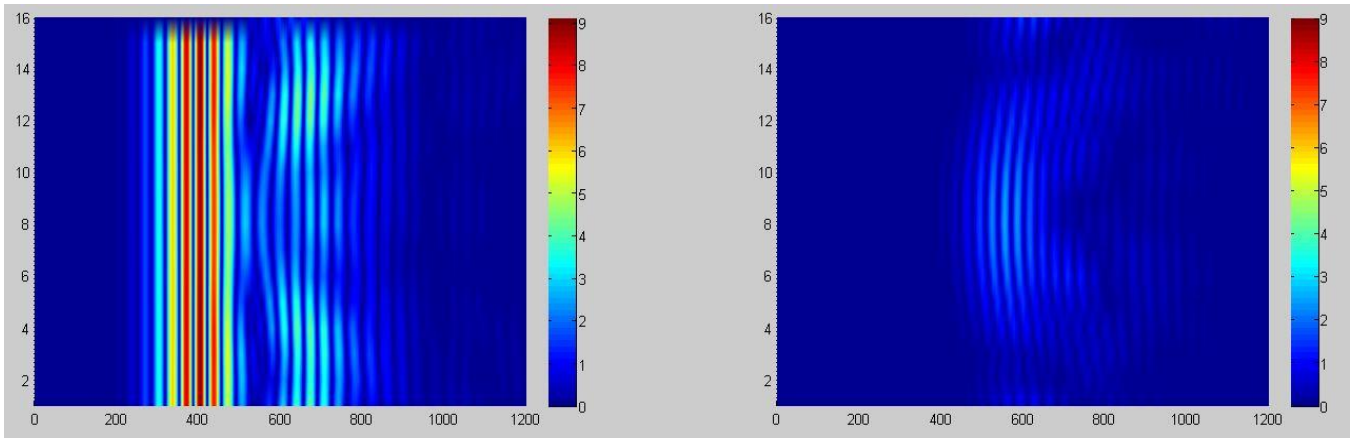

Fig.32 GPR image for the cylinder at 150 mm depth

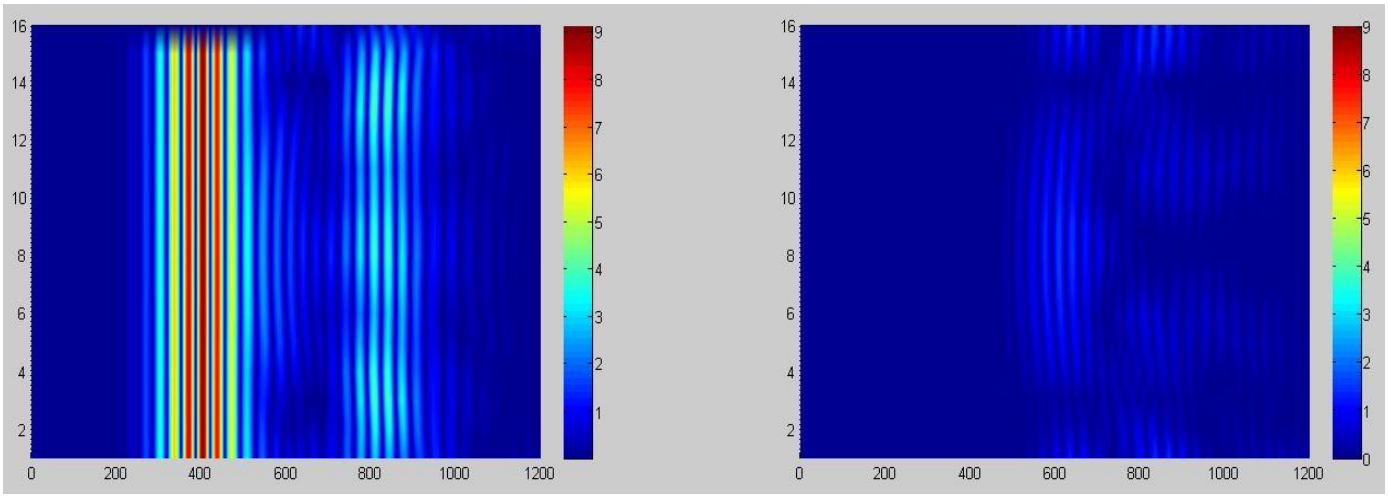

Fig.33 GPR image for the cylinder at 200 mm depth

Results of the simulation show a clear attenuation in the signal received with increasing depth, as well as a slight modification to the hyperbolic shape.

We can deduce that it's of a high importance to apply filters and reverse algorithms to the image to make it a reliable footprint or unique identifier of that target.

7.2. Rectangular target

The same work has been done for rectangular target

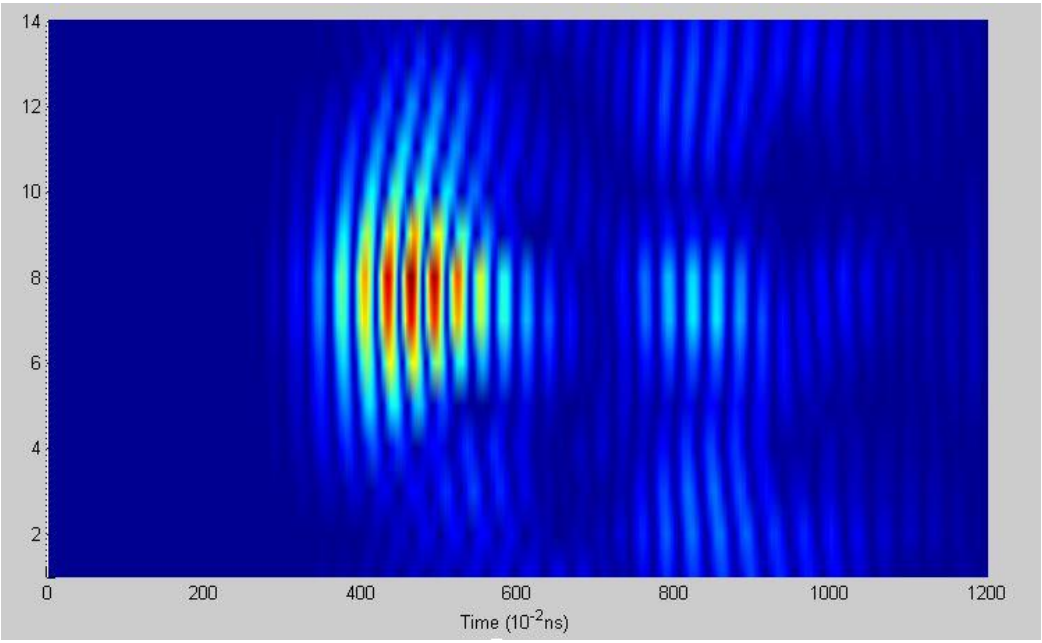

Fig.34 GPR image for the rectangular target at 50 mm depth

This result proves that each shape has a unique GPR image that would be essential for the recognition system as an identifier for that specific shape.

7.3. Two rectangular targets (Resolution test)

For the two rectangular targets 50x50 mm placed aside of each other in the scan direction and separated by 100 mm distance we get the following results

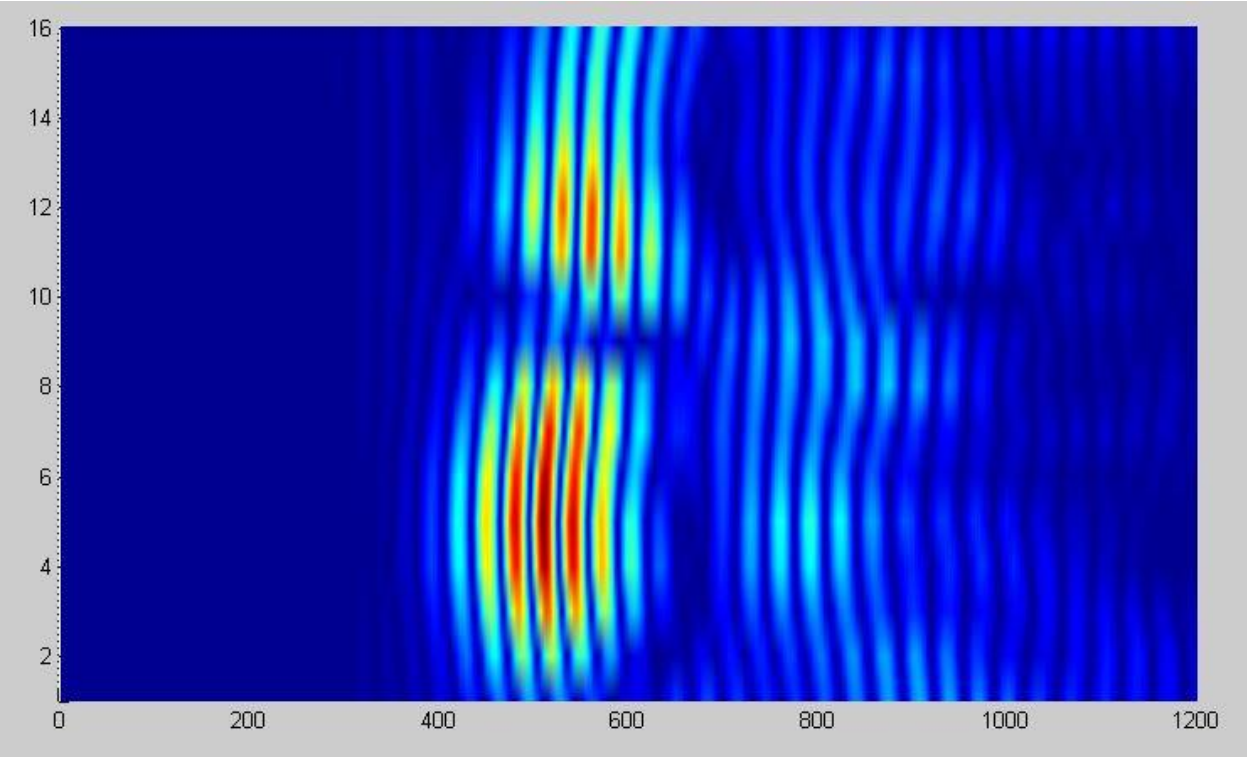

Fig.35 GPR image for two rectangular targets separated by 100 mm

Two separate objects are observed in this image that indicates without doubt the existence of two targets. But when we decrease the distance to 50 mm the two images will interfere and cannot be seen as separate targets.

This resolution is acceptable in the practical case though, where the landmines are buried in a sandy (no clays around) spots and separated by a distance fairly bigger than 10 cm.

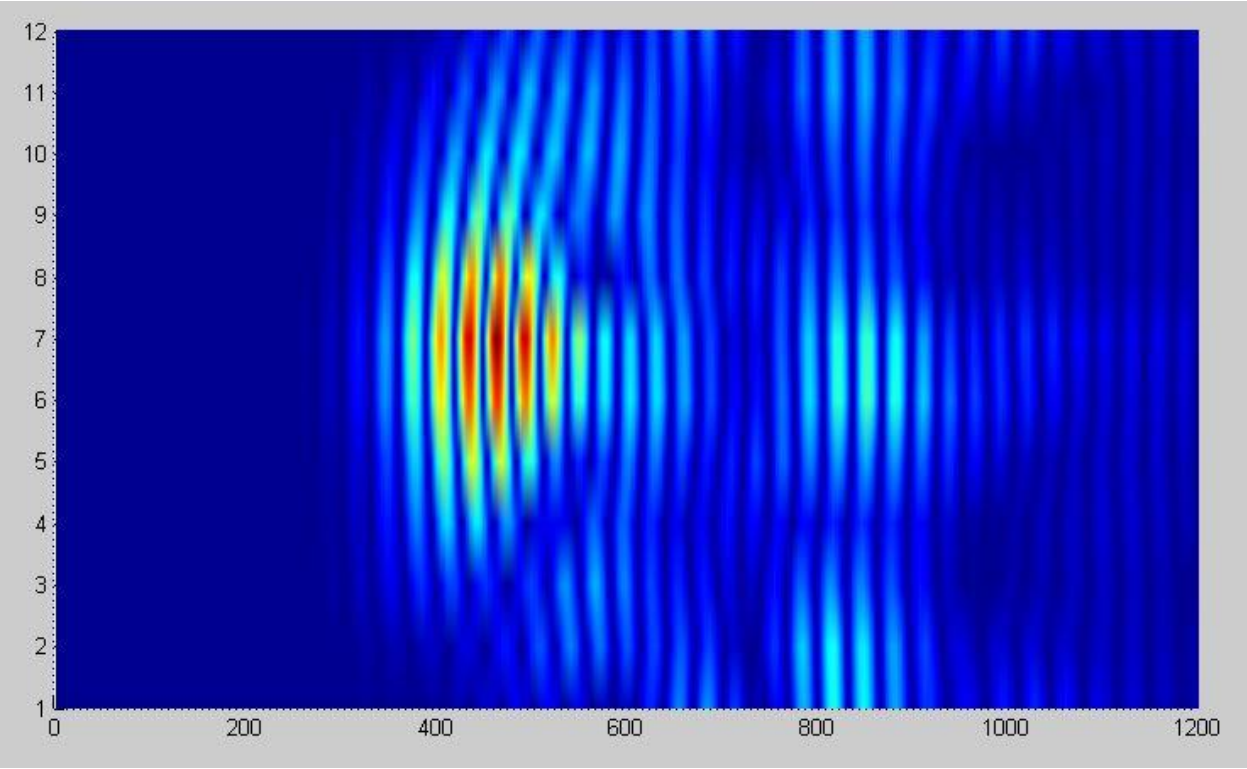

Fig.36 GPR image for 2 separate targets by a 50 mm distance

The results we got allow us to go further in the project and start collecting data for the learning process in the recognition system.

8. Data aquisition

The recognition system has to be able to distinguish between desired targets (landmines) and cluster targets such as rocks and other buried objects. For this purpose it is important to provide that system with GPR images that are expected to be received from landmines.

We gathered most encountered landmines in Lebanon and made 3d models of them.


Fig.37 Landmines encountered in Lebanon

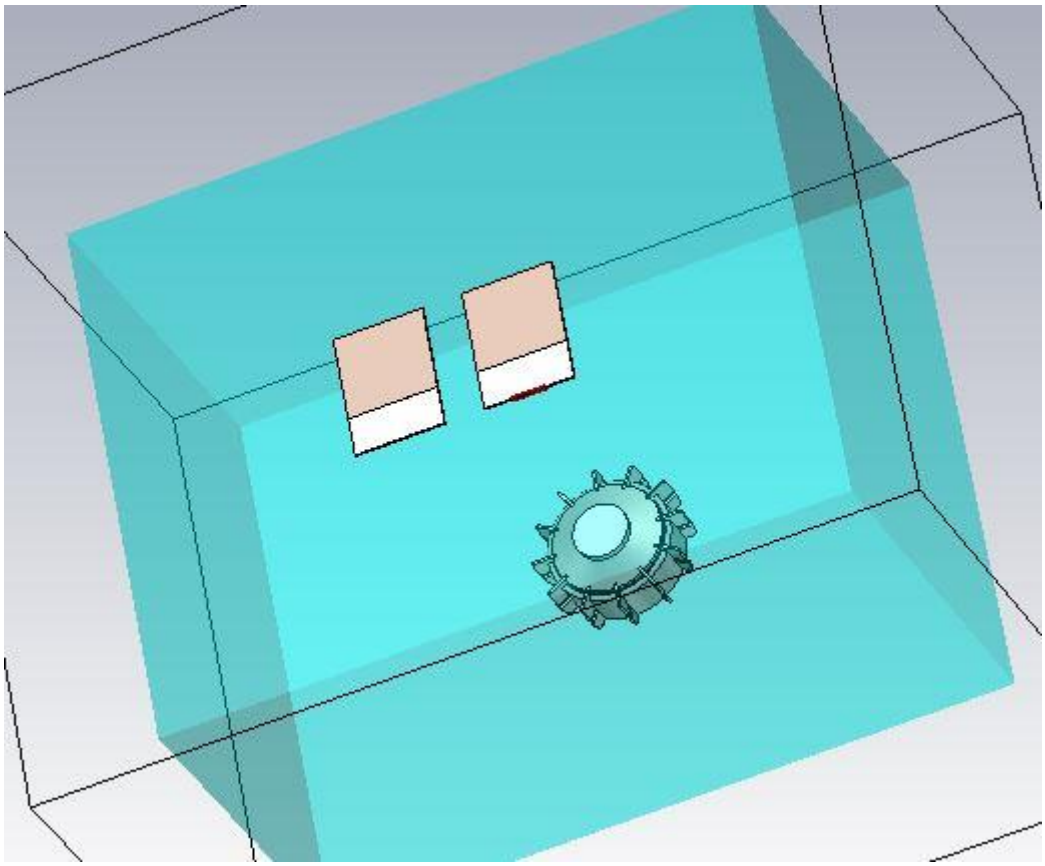

Fig.38 Landmine model in simulation

This stage of the project is still ongoing, and we are aiming to run simulations on different mines compositions such as detonators and explosive material due to the existence of mines made from plastic materials that allow the EM wave to propagate inside, and disturb the scattered signal.

CHAPTRE III: CONCLUSION AND FUTURE WORK

In this study simulations were done to test the power attenuation in different soil models and how it changes with the change of different factors such as moisture content and angle of incidence. Results showed that attenuation in the soil types studied is relatively similar as long as the moisture content is low, which is the practical case in demining process. This result can give us a fair estimation of the exposure time needed to reach a necessary temperature for the neutralization in a specific depth, by just taking the average electrical properties of the studied soil types. Ignoring the reflection coefficient, the best angle of incidence is 90 degree (normal incidence).

Concerning the GPR, an efficient system was constructed (cheap with acceptable gain and directivity), and simulations were done to get the cross section (2D image) of buried objects that have different geometric forms. The results insure that each geometric shape has a unique image which would help in the recognition system, but the image gets slight modifications with depth variation which we believe it could be removed if the correct algorithms were applied by the recognition system. The designed GPR shows a good resolution, as well as an ease in manufacturing and handling.

The project is still ongoing, as the data base for the recognition system is being built from landmines images. And it is expected to encounter some obstacles in the real practice.

LIST OF FIGURES

LIST OF TABLES

LIST OF SYMBOLS

1. τ : transmission coefficient.
2. Γ : reflection coefficient.
3. p_v : volumic charge density.
4. σ : electrical conductivity.
5. ϕ and θ : angles.
6. Λ : wavelengh.
7. E : electric field.
8. H : magetic field.
9. ω : angular velocity.
10. μ : magnetic permeabiliy.
11. ε : electrical permitivitty.
12. γ : propagation constant.
13. α : attenuation factor.
14. β : the phase constant.
15. η : medium impedence.
16. n : refractive index.
17. v : volume.
18. c_p : specific heat.
19. T : temperature.
20. t : time.
21. m : mass.
22. ρ : volumic mass.

INDEX

1. I.Hajnsek, K.papathanassiou, january 2005, Rough surface scattering models.

2. R. Prakash, D. Singh, and N. P. Pathak, The effect of soil texture in soil moisture retrieval for specular scattering at C-band, Department of Electronics & Computer Engineering
   Indian Institute of Technology Roorkee, Roorkee 247667, India.

3. FAWWAZ T. ULABY, PERCY P. BATLIVALA, MYRON C. DOBSON, Microwave Backscatter Dependence on Surface Roughness, Soil Moisture, and Soil Texture: Part 1I-Bare Soil.

4. John O. Curtis, Charles A. Weiss, Jr., Joel B. Everett, Effect of Soil Composition on Complex Dielectric Properties, US Army Corps of Engineers, Waterways Experiment Station.

5. Mohammed Al-Husseini, Ali El-Hajj, and Karim Y. Kabalan, A 1.9−13.5 GHz Low-Cost Microstrip Antenna, ECE Department, American University of Beirut.